



How well do global burned area products represent fire patterns in the Brazilian Savannas biome? An accuracy assessment of the MCD64 collections



Julia A. Rodrigues^a, Renata Libonati^{a,b,*}, Allan A. Pereira^c, Joana M.P. Nogueira^d,
Filippe L.M. Santos^a, Leonardo F. Peres^{a,e}, Ananda Santa Rosa^f, Wilfrid Schroeder^g,
José M.C. Pereira^b, Louis Giglio^h, Isabel F. Trigo^e, Alberto W. Setzer^d

^a Departamento de Meteorologia, Universidade Federal do Rio de Janeiro, 21941-916, Rio de Janeiro, RJ, Brazil

^b Centro de Estudos Florestais, Instituto Superior de Agronomia, Universidade de Lisboa, 1349-017, Lisboa, Portugal

^c Instituto Federal de Ciência e Tecnologia do Sul de Minas Gerais, 37890-000, Muzambinho, MG, Brazil

^d Centro de Previsão de Tempo e Estudos Climáticos/Instituto Nacional de Pesquisas Espaciais, Programa de Monitoramento de Queimada por Satélites, 12227-010, São José dos Campos, SP, Brazil

^e Instituto Português do Mar e da Atmosfera, 1749-077, Lisboa, Portugal

^f Departamento de Geografia, Universidade de Brasília, 70910-900, Brasília, DF, Brazil

^g Satellite Analysis Branch, NOAA/NESDIS, College Park, MD, 20740, USA

^h Department of Geographical Sciences, University of Maryland, College Park, MD, 20742, USA

ARTICLE INFO

Keywords:

Cerrado
Burned area
MODIS
MCD64
Validation
Satellite remote sensing

ABSTRACT

Knowledge about the current fire dynamics in the Brazilian Savannas (Cerrado) relies heavily on satellite-derived burned area (BA) products applied at the biome level. Nevertheless, there is still a lack of studies analyzing the consistency of available available satellite products concerning BA location and extension for the region. Accordingly, we performed an accuracy assessment of the MODerate resolution Imaging Spectroradiometer (MODIS) collection 6 BA product (MCD64 /C6) over 222,768,000 ha encompassing the Brazilian Cerrado. We used reference data derived from Landsat-8 OLI to perform an intercomparison of MCD64/C6 with 1) the previous collection 5.1 (C5.1); 2) independent active fires from the Visible Infrared Imaging Radiometer Suite (VIIRS); and 3) recent land use patterns. The results of the comparison between C6 and C5.1 indicate that the new collection decreases the omission error in 90% of the analyzed area and increases the burn hits, providing improved BA estimates in 61% of the region. However, the MCD64 product increases the overall commission errors in 74% of the area. The MCD64/C6 product showed a high coefficient of correlation with active fires independently detected by VIIRS ($\tau = 0.74$). For both MCD64 collections 5.1 and 6, the different accuracy assessment measures exhibited a marked performance deterioration from the north towards the south. The largest burn scars and total affected areas occur mainly across the northern Cerrado, explaining the better performance in that area. Conversely, greater inaccuracies were found in the southern Cerrado area, where natural vegetation has been converted into pasture and cropland, leading to fragmented landscapes and small fire patches. Finally, the BAs mapped by both collections were similar in location albeit divergent in the magnitude, with C6 detecting 21% more area than C5.1 during the year 2015.

1. Introduction

The Brazilian Cerrado, the largest savanna ecosystem in the world, is a very relevant biome due to its large geographic extent, high levels of

biodiversity, and influence on global biogeochemical cycles (Franco et al., 2014). The species richness is greater than that of other biomes, including the Amazon, due to the heterogeneous vegetation structure, and it is thus considered a biodiversity hotspot for conservation

* Corresponding author at: Departamento de Meteorologia, Universidade Federal do Rio de Janeiro, 21941-916, Rio de Janeiro, Brazil.

E-mail addresses: lasa@igeo.ufrj.br (J.A. Rodrigues), renata.libonati@igeo.ufrj.br (R. Libonati), allan.pereira@ifsuldeminas.edu.br (A.A. Pereira), joana.nogueira@inpe.br (J.M.P. Nogueira), filmaias@ufrj.br (F.L.M. Santos), leonardo.peres@igeo.ufrj.br (L.F. Peres), ananda.santarosa@aluno.unb.br (A. Santa Rosa), wilfrid.schroeder@noaa.gov (W. Schroeder), jmcpereira@isa.ulisboa.pt (J.M.C. Pereira), lgiglio@umd.edu (L. Giglio), isabel.trigo@ipma.pt (I.F. Trigo), alberto.setzer@inpe.br (A.W. Setzer).

<https://doi.org/10.1016/j.jag.2019.02.010>

Received 7 January 2019; Received in revised form 18 February 2019; Accepted 18 February 2019

Available online 28 February 2019

0303-2434/ © 2019 Elsevier B.V. All rights reserved.

priorities (Myers et al., 2000). The Cerrado presents fire-dependent vegetation that evolved in the presence of recurrent natural fires, which maintain its biodiversity (Hoffmann, 2002; Pivello, 2017). Many species are adapted to this regime needing fire for seed germination and colonization (Beerling and Osborne, 2006; Dantas et al., 2013; Miranda et al., 2009). This biome has suffered from the loss of habitats and ecosystem services, with 43% (88 Mha) of its natural vegetation having been converted into pasture and croplands in recent decades (Strassburg et al., 2017). These anthropogenic activities still use fire as a tool for land clearing, pasture renewal and expansion (Araújo et al., 2012; Beuchle et al., 2015; Chen et al., 2013b; Durigan and Ratter, 2016; Gomes et al., 2018; Klink and Machado, 2005; Pivello, 2017). Land cover changes in conjunction with climate variability have the potential to induce vegetation burning, thereby impacting vast areas (Song et al., 2018). Furthermore, positive feedbacks among land use, climate variability, and ecosystem responses may increase biome degradation through enhanced fire occurrence (Archibald and Lehmann, 2018; Santín and Doerr, 2016). The use of fire in the Cerrado requires accurate characterization of the phenomenon in order to promote sustainable land management practices that can maximize services without compromising ecosystem resilience (Carranza et al., 2014; Durigan and Ratter, 2016; Pivello, 2017; Santín and Doerr, 2016).

Accordingly, many satellite-derived burned area (BA) products have been developed for fire monitoring, modeling, and risk assessments (Mouillot et al., 2014). In the early 2000s, the MODerate resolution Imaging Spectroradiometer (MODIS) aboard the Terra and Aqua satellites from the National Atmospheric Space Agency (NASA) were the first moderate-resolution (~1 km) sensors to include dedicated channels enabling routine global fire observations. The MODIS sensors have been successfully used for active fire monitoring (Giglio et al., 2016b), BA mapping (Boschetti et al., 2015; Chuvieco et al., 2008; Giglio et al., 2009; Libonati et al., 2015; Panisset et al., 2017; Ramo and Chuvieco, 2017; Randerson et al., 2012; Roy et al., 2005), and fire model benchmarking in many regions around the globe (Hantson et al., 2016; Nogueira et al., 2017a). The MODIS burned area product (MCD64) collection 5.1 released in 2012 has been widely used in numerous studies examining fire regimes and biomass burning emissions (Andela et al., 2017; Chen et al., 2013a; Chuvieco et al., 2014; Zhang et al., 2016).

Different global and regional studies have evaluated satellite-derived BA products, showing their strengths and weaknesses (Mouillot et al., 2014). A global BA accuracy assessment identified MCD64 C5.1 as more accurate than the MODIS MCD45 C5.1 and the Envisat/MERIS-based products, even if the MCD64 C5.1 exhibited substantial underestimation of the total BA in different vegetation types (Alonso-Canas and Chuvieco, 2015; Padilla et al., 2015; Roy et al., 1999). In boreal Eurasia, the MCD64 C5.1 product was demonstrated to be inadequate for small fire detection (Zhu et al., 2017), in particular those associated with cropland burning (Fornacca et al., 2017; Hall et al., 2016). Over South Africa, the same drawbacks were found, but MCD64 C5.1 showed higher detection probabilities relative to the MCD45 C5.1 product for BA fractions > 50% within the MODIS pixel (Tsela et al., 2014, 2010). In the northern Brazilian savannas, the MCD64 C5.1 BA estimates for the 2005–2010 period were 70% lower than estimated by independent reference data, while showing similar temporal variability (Libonati et al., 2015). Omission errors were also reported in southern Brazilian savannas, where small burns dominate the fire size distribution (Pereira et al., 2017). In April 2018, the Land Processes Distributed Active Archive Center (LP DAAC) decommissioned MCD64 C5.1 and released collection 6 (hereafter C6), which is a reprocessed version including updated calibration and geolocation information in addition to algorithm upgrades (Giglio et al., 2018). A comparison between the MCD64 C5.1 and C6 products for 2002–2016 (Giglio et al., 2018) showed improved performance over small fires, especially in croplands, increasing the average BA mapped worldwide by 26% (except in the Boreal region where a 6% reduction was observed in the areas mapped). Compared to

previous versions, MCD64/C6 has an improved characterization of the date of burning, lower omission error (37% vs. 40% for MCD64 C5.1, and 45% for MCD45 C5.1), and lower relative bias of -17.9% compared to MCD64 C5.1 (-22.7%) and MCD45 C5.1 (-27.9%). However, MCD64 C6 presented a higher commission error (24% vs. 22% and 23% for MCD64 C5.1 and MCD45 C5.1, respectively) and an overall accuracy of 97%, similar to the old collections.

Despite the large fire activity in the Cerrado, there is still a lack of studies analyzing the consistency among currently available BA products for the region that take into account the BA location and extension and that include the most recent MCD64 C6 product. The majority of studies based on MCD64 C5.1 data for the Brazilian Cerrado have been performed on a few limited areas mainly composed of conservation units (Araújo and De Ferreira, 2015; Libonati et al., 2015; Nogueira et al., 2017b; Pereira et al., 2017; Santos et al., 2018). Moreover, little is known about errors in remotely sensed BA products as a function of land use/cover in the Cerrado. Although some studies have focused on the impact of land cover changes on the BA product uncertainties (Araújo et al., 2012), only small areas were analysed. Accordingly, in this work we performed a rigorous assessment of MCD64 C5.1 and the new MCD64 C6 for the Brazilian Cerrado at the biome scale, using reference burn scars based on United States Geological Survey Landsat 30 m resolution data for the 2015 fire season, a year with extensive BA in the Cerrado biome (Pereira et al., 2017). Complementing the analyses, we performed a comparison with active fires independently detected by the Suomi-National Polar-orbiting Partnership Visible Infrared Imaging Radiometer Suite (VIIRS) from 2013 to 2016, assuming that they provides a reasonable, complementary and practical approximation of the performance of MCD64 BA collections, allowing wall-to-wall temporal and spatial coverage which is unfeasible with Landsat-based validation practices. Finally, we analyzed land use patterns as an explanatory source of uncertainties from MCD64 collections.

2. Data and methods

2.1. Study area

The Brazilian Cerrado (2°20'25"S to 24°41'5"S and 60°06'34"W to 41°31'18"W) covers 204,500,000 ha and dominates most of central Brazil (Fig. 1). The predominant climate is tropical with a dry winter (Aw type in Koppen's classification) (Alvares et al., 2014; Kottek et al., 2006), and with high inter-annual variability in precipitation, ranging from 800 to 2000 mm per year (Ratter et al., 1997). The dry season occurs from the end of June to mid-October, when fire incidence is highest in this biome (Libonati et al., 2015; Nogueira et al., 2017b; Silva et al., 2016). The typical vegetation communities range from closed and open shrublands, to open savannas and natural grasslands, and including open deciduous canopy forests (Fig. 1). This variation is determined by a mosaic of different soil types, irregular water availability, burn regimes, land use, and topographic variations (DaSilva and Bates, 2002). The Cerrado is also experiencing significant land use change, with its native vegetation being replaced by exotic grasslands and croplands for livestock and intensive agriculture in recent years (Fig. 1) (Lapola et al., 2014; Sano et al., 2010; Song et al., 2018).

2.2. Datasets

In this study, we evaluate the MODIS BA MCD64 product, released as Collection 5.1 and 6 (hereafter C5.1 and C6, respectively), using burned scars from Landsat as our reference. The active fires and land cover information are used as auxiliary data to discuss the results. All datasets are described below.

2.2.1. An overview MODIS burned area products

The MCD45 product (Roy et al., 2005) was the first BA product developed by NASA using data from the MODIS sensors onboard the

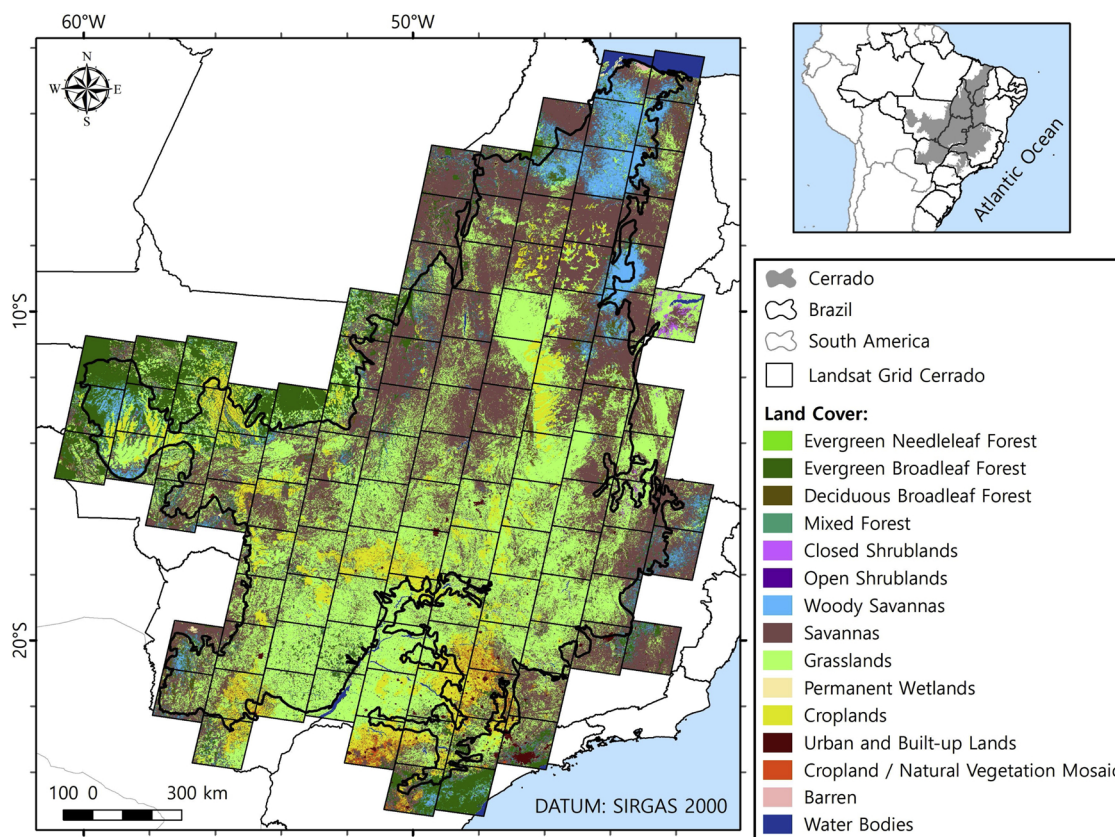


Fig. 1. Land cover distribution in the study area in the year 2015 derived from the MCD12Q1 MODIS C6 product with 15 classes defined by the International Geosphere-Biosphere Programme (IGBP) land cover classification scheme (Loveland and Belward, 1997).

Terra and Aqua satellites. The MCD45 algorithm is based on a model that accounts for directional reflectance effects and temporal changes in the land surface properties (Roy et al., 2008). The product provides the burn date together with a quality control layer (hereafter quality flag - QF), which indicates the confidence level of the burn detection. The MCD45 and MCD64 C5.1 products were decommissioned in April 2018, and subsequently replaced by MCD64 C6 in August 2018.

MCD64 maps BA on a daily basis globally at 500 m spatial resolution by combining MODIS surface reflectance imagery, active fire data, and ancillary vegetation cover information. The mapping algorithm uses active fire observations to develop a statistical characterization of burn-related and non-burn-related change during the mapping period, and subsequently employs Bayes' rule, supplemented with additional probabilistic tests, to classify individual grid cells as either burned or unburned. The algorithm has been applied to the full archive of MODIS fire data, yielding a monthly global BA product spanning the period from late 2000 through the present. Collections 5.1 and 6 from MCD64 are freely available from the LP DAAC (<https://lpdaac.usgs.gov/>) and several public FTP servers (see <http://modis-fire.umd.edu/ba.html>).

Tiles for MCD64 over the study area (Fig. 1) were mosaicked and remapped using the Modis Reprojection Tool (MRT) (https://lpdaac.usgs.gov/tools/modis_reprojection_tool). The product in a global sinusoidal projection contains five data layers (Burn Date, Burn Date Uncertainty, Quality Assessment, First Day, and Last Day), each stored as a separate HDF4 Science DataSet (SDS) file format.

2.2.2. Landsat sensor-derived burned scars and the study samples

We used burned scars derived from Landsat images as reference data in this study. The reference scars were mapped every 16 days at a spatial resolution of 30 m using multispectral images from the Thematic Mapper (TM) and Operational Land Imager (OLI) sensors aboard the Landsat-5 (L5) and 8 (L8) satellites, respectively. The thematic maps are

systematically generated by the National Institute for Space Research (INPE) and are available at <https://prodwww-queimadas.dgi.inpe.br/aq30m/#> (Melchiori et al., 2014). The BA classification method is based on the Normalized Difference Vegetation Index (NDVI) and Normalized Burn Ratio Long-shortwave infrared variation (NBRL) indices, and on change detection between consecutive images of both indices. The dataset includes burned scars for the entire Cerrado biome from 2001 until the present. The burnt scars automatically generated by INPE's algorithm are further subject to an independent *in situ* analysis and visual photo interpretation.

A series of quality control procedures for removing data of reduced accuracy were applied here to ensure consistency among all the burn scar samples. Five burn scar selection criteria defined by the validation protocol recommended by the Committee on Earth Observations (CEOS) Land Product Validation Working Group (Boschetti et al., 2010) were used here to filter reference burn scars in order to minimize errors, namely:

- I) Use of a temporal separation of 16 days between consecutive images (the minimum possible time difference for Landsat) to avoid spectral signal attenuation;
- II) Exclude months outside the June-to-November period to reduce cloud contamination and rainfall episodes;
- III) Confine the analysis to scenes with cloud coverage equal to or less than 10%;
- IV) Perform a detailed analysis of cloud distribution in pre- and post-fire images with associated scars to avoid commission errors;
- V) Exclude scars smaller than 25 ha, corresponding to the minimum area of one MCD64 pixel.

After applying the criteria above, the initial 113 path/row scenes were reduced to 84 scenes, which were further visually inspected by an

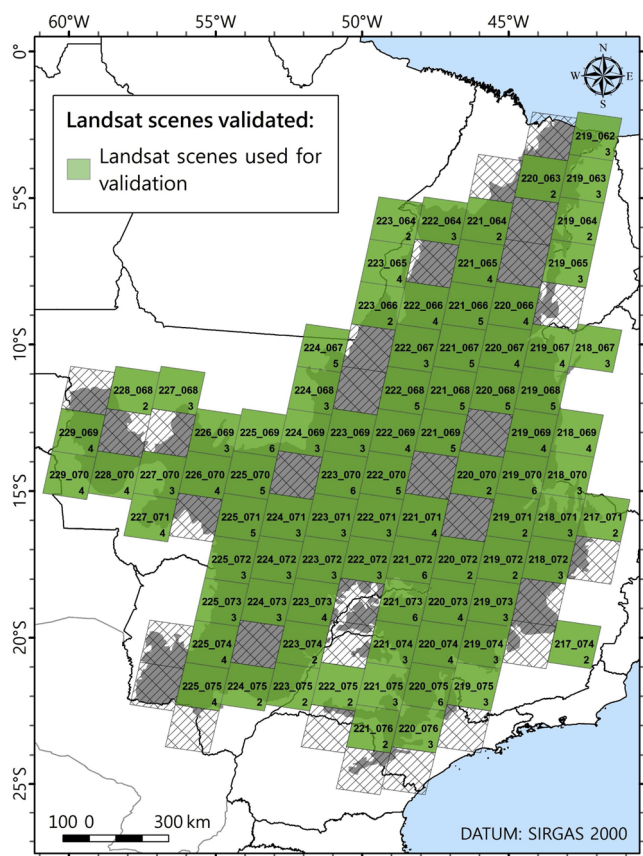


Fig. 2. Spatial distribution of the 84 Landsat reference scenes in the Cerrado biome. The number in each scene corresponds to the path and row in the Worldwide Reference System (WRS-2). The numbers below each path/row represent the number of images used to compose the validation period of each Landsat scene.

independent analyst to ensure quality of the reference maps (Fig. 2). The initial and final validated period was further extended by two days due to burn date uncertainty (Giglio et al., 2016a). Accordingly, the accuracy assessment was performed for the 84 Landsat selected scenes during 2015, a year with extensive BA in the Cerrado biome (Pereira et al., 2017).

2.2.3. Auxiliary datasets

2.2.3.1. VIIRS active fires. We performed a temporal and spatial comparison of MODIS BA products with the VIIRS 375-m active fire product (VNP14IMG) (Schroeder et al., 2014) over the Cerrado biome for the 2013–2016 period. We chose the VIIRS fire active product because these data are independent of the MODIS fire active data used in the MCD64 algorithm. Moreover, the VIIRS 375-m active fire product provides the best possible compromise between spatial and temporal resolution of currently available operational satellite fire data sets for use in support of burned area identification. Its performance is proven superior compared to other operational satellite active fire products, while providing systematic 12 h observations of the entire globe. Other active fire data sets may be available although limitations involving their spatial/temporal information and/or operational status/accessibility prevented their use here (e.g., GOES-East, AVHRR/Metop series, Sentinel-3).

The VIIRS 375-m active fires data have been validated over distinct fire-prone ecosystems, revealing a higher fire detection rate compared to MODIS 1-km data (Csiszar et al., 2014; Oliva and Schroeder, 2015; Schroeder et al., 2014). The results of the validation over tropical grassland and savannas and over agricultural fires revealed that the omission errors associated with fire affected area estimation decrease

with increased fire size, although high fire spread rates can reduce the efficacy of fire perimeter delineation using VIIRS active fire detections (Oliva and Schroeder, 2015). The statistical representativeness of the VIIRS active fire detections in the Cerrado biome was assessed here by comparing summary statistics over each one of the 84 Landsat scenes during the 2015 dry season. The two datasets present very similar behavior as indicated by the value of 0.72 for the Kendall rank coefficient (τ), statistically significant at the 0.05 level. The VNP14IMG product has a resolution of 375 m and is currently available from 2012 until present; the data were downloaded in shapefile format from <https://firms.modaps.eosdis.nasa.gov/download/>.

2.2.3.2. Land use data. We conducted a spatial regional-scale analysis aiming to shed light on the relationships between BA characteristics (main patterns and uncertainties) and land use. The approach was performed using the updated collection 6 Land Cover Type Yearly Global 500-m MCD12Q1 product (Friedl et al., 2010). The MCD12Q1 C6 product incorporates 13 data layers and five different classification schemes derived through a Random Forest Classifier with a new legend based on a nested set of classifications (Sulla-Menashe and Friedl, 2018). In this study, we used the layer following the International Geosphere-Biosphere Programme (IGBP) land cover classification scheme (Loveland and Belward, 1997) for 2015. The IGBP classification has 17 land cover classes, of which 15 occur in the Cerrado biome, as shown in Fig. 1. The tile grids corresponding to the Cerrado region were downloaded from the Earthdata search from NASA (<https://search.earthdata.nasa.gov/>) and projected to datum SIRGAS 2000 EPSG:4674, the geodetic reference system for South America. MCD12Q1 C6 was used here at the original spatial resolution (500 m) to evaluate the influence of land use on BA in the Cerrado.

In order to assess these impacts on burnt area distribution, we categorized each of the 84 Landsat scenes according to the degree of land use using a conceptual clustering. Land use intensity (LUI) was characterized by the presence of pixels belonging to the MCD12Q1-IGBP C6 Grasslands, Croplands and Cropland/Natural Vegetation Mosaic land cover classes from the 2015 map. In accordance with the IGBP classification (Loveland and Belward, 1997), the Grasslands class is dominated by annual herbaceous plants (< 2 m), the Croplands class refers to areas with at least 60% of cultivated cropland, and the Cropland/Natural Vegetation Mosaic class are mosaics of small-scale cultivation (40–60%) with natural trees, shrubs, or herbaceous vegetation. We defined three different LUI levels for individual Landsat scenes, with the following thresholds: 0–50% (low LUI), 51–75% (medium LUI), and 76–100% (high LUI).

2.3. Methodology

In contrast to previous BA accuracy assessments in the region, the current work aims to perform an assessment and intercomparison over the whole Cerrado biome at different geographical levels, namely, the local, regional, and biome levels, taking into account land cover and land use patterns in the region.

2.3.1. Local accuracy assessment

The evaluation of non-probabilistic burned/unburned area detection is usually performed through a cross tabulation between the burned and unburned classification and a reference data set and using scalar attributes and skill scores describing the 2 × 2 contingency table (Lillesand and Kiefer, 1994) (Table 1). The validation procedure assumed here was, however, performed using a statistical technique called the *low-resolution bias concept*. This technique takes into account the fraction of area burned within the MODIS BA product pixel (500 m) quantified by the reference map (Landsat-derived), in accordance with the methodology proposed by Boschetti et al. (2004) and already used in other studies (Libonati et al., 2015; Padilla et al., 2014).

Four accuracy assessment measures, including the Threat Score

Table 1
Contingency table for classified burned areas between the Landsat reference map and the MCD64 BA products (C5.1 and C6).

		Reference map (Landsat-derived)		
		Burned	Unburned	Total
Burned area product evaluated (MCD64)	Burned	a	b	a + b
	Unburned	c	d	c + d
	Total	a + c	b + d	a + b + c + d

a = pixels classified as burned in the reference map and in the BA product.
 b = pixels classified as unburned in the reference map and as burned in the BA product.
 c = pixels classified as burned in the reference map and as unburned in the BA product.
 d = pixels classified as unburned in the reference map and in the BA product.

(TS), Bias (B) and Commission (CE) and Omission (OE) errors, were derived from the contingency table. The threat score TS (Eq. (1)) is an index used in the analysis of rare events, which considers only the occurrence of the event (in this case, burning). The bias B (Eq. (2)) shows whether the product underestimates ($B < 1$) or overestimates ($B > 1$) the total BA. The CE (Eq. (3)) is the fraction of pixels mistakenly classified as burned, unlike the OE (Eq. (4)), which is the fraction of burned pixels not detected by the product. The CE and OE range between zero and one, where values close to zero indicate the best measures.

$$TS = \frac{a}{a + b + c} \tag{1}$$

$$B = \frac{a + b}{a + c} \tag{2}$$

$$CE = \frac{b}{a + b} \tag{3}$$

$$OE = \frac{c}{a + c} \tag{4}$$

2.3.2. Regional and temporal analysis with active fires

A regional approach with the support of active fire information is used here to verify the spatial and temporal consistency of the BA product variability, as commonly done in previous studies (Boschetti et al., 2010; Giglio et al., 2010). Active fire information provides a direct indication of fire occurrence, generally retrieved with low false-alarms rates (Giglio et al., 2016b; Schroeder et al., 2008). This type of comparison provides useful information about the performance the BA product in large areas and periods in which no other reference data are available to perform an accuracy assessment (Humber et al., 2018). This is the case for the Landsat reference BA information from INPE, which is restricted to the fire season. Active fires were also used here to analyze the temporal consistency of the BA products at the biome level in terms of the interannual variability.

To assess the spatial accuracy at the regional scale, we compared the MCD64 C5.1 and C6 collections with the VIIRS active fires by computing the total annual amount of BA and of active fire in each 25 x 25 km grid cell. The nonparametric Kendall rank coefficient (τ) was used to assess the correlation between the MCD64 collections and VIIRS active fires for each year of the period from 2013 to 2016, testing the null hypothesis (H0) of no positive correlation between BA maps and the active fire data. The alternative hypothesis (H1) indicates that of a positive correlation between BA and active fires, at a significance level of 0.05. This test is distribution-free and robust against noise, in contrast to the traditional ordinary least squares-based methods (Wilks, 2011).

3. Results

In this section, we present the statistical analysis of the accuracy assessment measures from the contingency table. Fig. 3 shows the spatial patterns of all four measures for both MCD64 collections (C5.1 and C6), together with the respective differences between the collections. These spatial patterns clearly reveal a well-defined north-south gradient for all three accuracy measures (i.e., TS, OE, and CE). The best results for TS, OE, and CE are concentrated in the northern part of the Cerrado (from latitude 2°S to 15°S or from Landsat row 062 to 070) for both collections (Fig. 3, i and ii), where the largest scars were observed (represented by the size of circles inside each scene). Conversely, a well-defined spatial pattern was not observed for B.

Although the TS of both collections exhibited a similar distribution and variability, C6 presents better (worse) results in 61% (28%) of the scenes, whereas no meaningful differences between the collections were observed in 11% of the scenes (Fig. 3a, iii). The overall improvement in TS is most likely related to the fact that OE decreased in 90% of the cases, increased in 5% and did not exhibit variation in the other 5% of the scenes (Fig. 3b, iii). The maps of the difference between the collections (Fig. 3, iii) indicate the predominance of positive (negative) changes for TS (OE), indicating improvements in C6 compared to C5.1. However, positive values of ΔCE were still observed for a few scenes, indicating an increase in CE in C6 (Fig. 3c, iii). Accordingly, the C6 data exhibited higher CE values compared to C5.1 for 74% of the scenes analyzed; only 14% of the scenes exhibited an improvement in C6. Also, C6 produced a higher BA totals according to the ΔB results, with 92% of the scenes exhibiting an increment, 5% exhibiting a decline, and 3% remaining constant (Fig. 3d, iii). C5.1 underestimates the BA in most scenes ($B < 1$), whereas C6 overestimates it ($B > 1$).

According to the analyses of CE and OE, the MCD64/C6 product provides lower OE and higher CE than C5.1. For the 84 validated scenes, our results indicate that on average the Cerrado biome presents a reduction of 6.8% in the OE and an increase of 1.3% and 5% in the TS and CE, respectively. To assess whether the observed difference between both collections is statistically significant, we performed a hypothesis test considering for the null hypothesis that the mean values of the accuracy assessment measures for the 84 analyzed scenes are the same for both collections. For all four accuracy assessment measures, the returned values rejected the null hypothesis at the 1% significance level.

In 2015, the BA estimated by both MCD64 collections was similar in location, albeit divergent in magnitude (Fig. 4). This is evident in the values of the total BA detected by MCD64 C6 (15,070,850 ha) compared to C5.1 (11,990,827 ha) (Fig. 4a and b), where the difference between them (C6 - C5.1) totals 3,080,023 ha (Fig. 4c). Regarding the spatial distribution, the highest BA for both the MCD64 C5.1 and C6 products was observed in the northern region of the Cerrado, similar to VIIRS active fires (Fig. 4d), highlighting the substantial difference in the north-south BA patterns. The observed agreement with active fires confirmed the ability of the updated C6 product to track the spatial patterns of BAs. Fig. 5 shows the BA values (C5.1 and C6) within a 25 x 25 km grid cell plotted against the corresponding VIIRS active fires for the 2013–2016 period and the respective Kendall correlation index. C6 exhibited a higher correlation with the VIIRS active fires data than C5.1. For C6, the highest Kendall's correlation index was found for 2014 ($\tau = 0.78$) and the lowest for 2016 ($\tau = 0.71$). The average value of Kendall's coefficient was 0.74, with a standard deviation of 0.033. For C5.1, the best result was found for 2014 ($\tau = 0.73$) and the worst for 2013 and 2016 ($\tau = 0.68$). In this case, the average value of τ was 0.70, with a standard deviation of 0.026. In all scatterplots, the regression line passes nearly through the origin, and the slopes are almost the same for both collections and all years.

The Cerrado biome covers a large area with strong BA spatial variability, and selection of groups or subsamples covering the regional distribution of BA is essential to minimize the overall accuracy

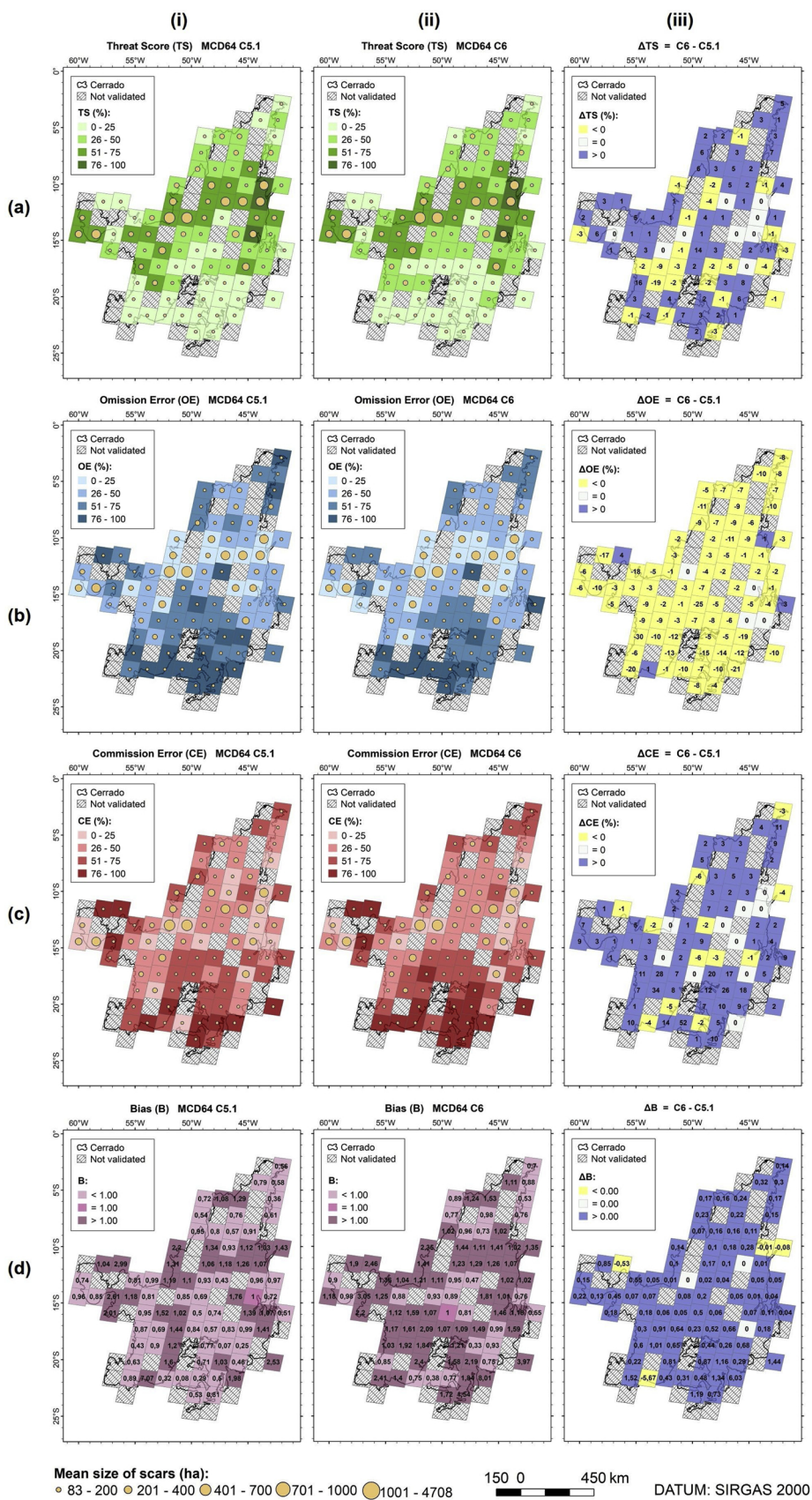


Fig. 3. Percentage of Threat Score – TS (a), Omission Error – OE (b), Commission Error – CE (c) and Bias – B (d) measurements of MCD64 (i) C5.1, (ii) C6 and (iii) the difference between the two collections ($\Delta = C6 - C5.1$). The light circles represent the mean size of scars obtained by the ratio between total burned area (in ha) and the number of scars validated, considering the dates selected in each scene.

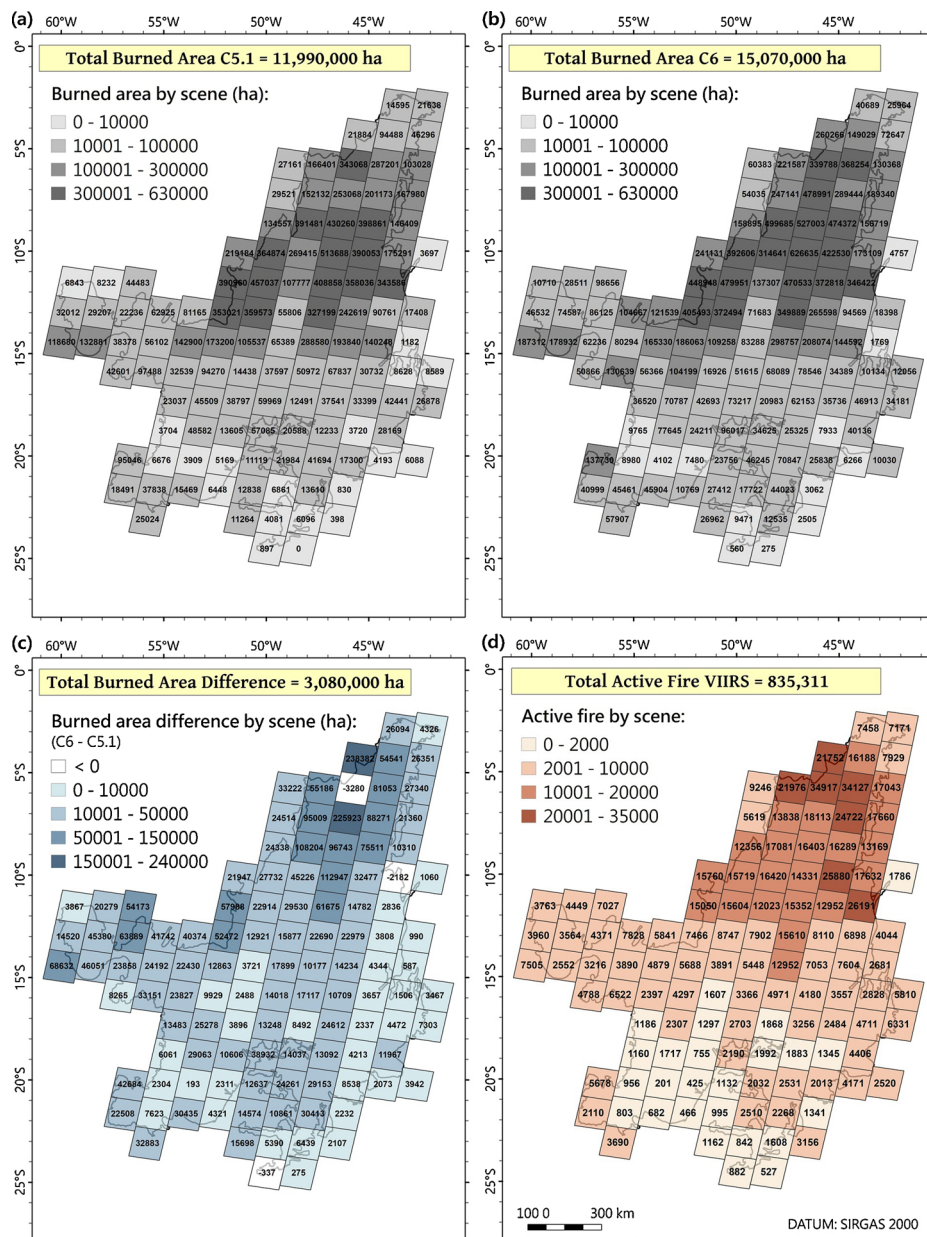


Fig. 4. Total burned area (BA, ha) in each Landsat path-row as detected by MCD64 C5.1 (a) and MCD64 C6 (b), the BA difference between C6 and C5.1 (c) and the total VIIRS active fires (d) in the Cerrado for 2015.

variance, thus guaranteeing reliability and representativeness of the validation results (Boschetti et al., 2016; Padilla et al., 2017). Accordingly, we stratified our study region into four groups according to the number of active fires (Fig. 4d). These groups were defined as follows: (a) Group 1 - 200–2000 VIIRS active fires, (b) Group 2 - 2001–10000 VIIRS active fires, (c) Group 3 - 10001–20000 VIIRS active fires and (d) Group 4 - 20001–35000 VIIRS active fires. Small scars (25–100 ha) are highly frequent (greater than 62%) in all VIIRS active fire groups and mainly in group 1, with 75% (Fig. 6, i). In contrast, large scars (100–1500 ha) are less frequent (between 25–35%), and mega scars (> 1500 ha) are very uncommon (less than 3%) for all groups. However, mega scars are responsible for most of the burned areas in groups 2–4 (greater than 50%), whereas for group 1, small and large scars contribute more (35% and 54%, respectively) than mega scars (11% (Fig. 6, ii).

Fig. 7 shows the stratified boxplots of the accuracy assessment measures (TS, CE, OE and B) for both collections, considering the 84 validated scenes within Cerrado as depicted in Fig. 2, according to the

number of active fires (VIIRS group 1, Group 2, Group 3, and Group 4). As the accuracy assessment measures from the contingency table consider each error in a generalized manner, we analyzed the overlaps between Landsat and MCD64 scars by taking into account the burned scars size per classes of 25–100 ha, 100–1500 ha, and > 1500 ha. In this manner, we can evaluate the ability of the algorithm to identify smaller burned patches, and quantify the false alarms and scar omissions. In general, the results from C6 not only exhibit a lower variability in terms of the four accuracy assessment measures, but also an increase in TS and decrease in OE and CE as the number of active fire increases (VIIRS groups from 1 to 4) (Fig. 7a–d, i). For both collections, OE is approximately 60–80% (20–30%) higher (lower) in areas classified as group 1 (group 4), with the lowest (highest) density of active fires. The C6 exhibits a slight improvement in TS and OE and a slight deterioration in CE. The TS, OE, and CE of C6 have smaller amplitudes than for C5.1 in all active fires groups, in groups 2 to 4, and only in group 1, respectively. Regarding the bias measurements, the C5.1 (6) collection generally underestimates (overestimates), median < 1.0 (median > 1.0),

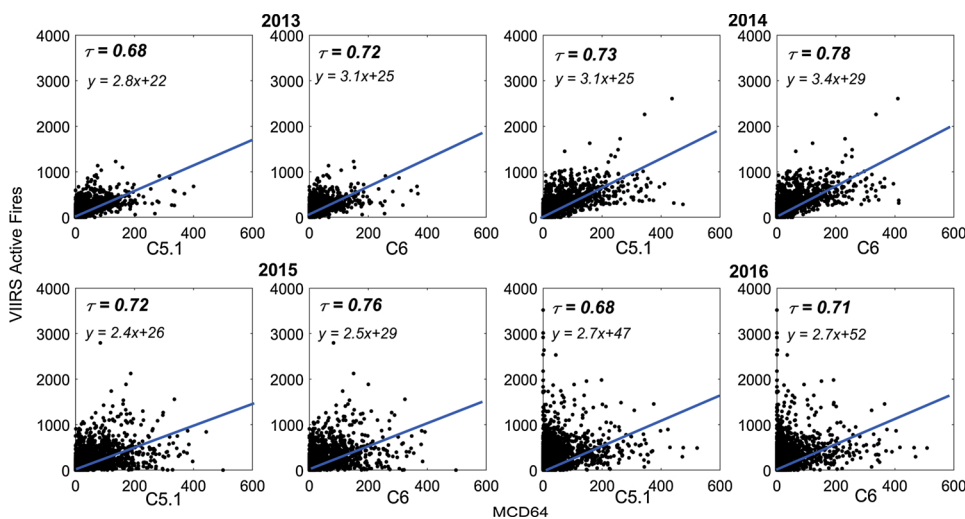


Fig. 5. Relationships between the total annual burned area (km²) from MCD64 collections C5.1 and C6 and total number of VIIRS active fires counts within a 25 × 25 km grid cell from 2013 to 2016. The regression line (in blue) and Kendall's coefficient are also displayed in each subplot. (For interpretation of the references to colour in this figure legend, the reader is referred to the web version of this article).

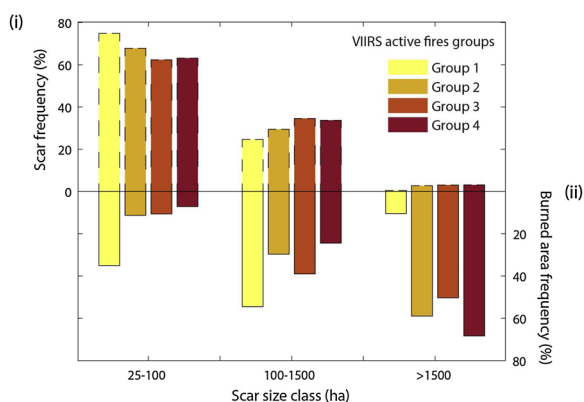


Fig. 6. Scar (% i, dashed bars) and burned area (% ii, solid bars) frequencies according to scar size classes (25–100 ha, 100–1500 ha and > 1500 ha) for each VIIRS Groups: Group 1 (200–2000 active fires, light yellow bars), Group 2 (2001–10000 active fires, dark yellow bars), Group 3 (10001–20000 active fires, orange bars) and Group 4 (20001–35000 active fires, red bars). (For interpretation of the references to colour in this figure legend, the reader is referred to the web version of this article).

the total BA in the groups 1, 2 and 3 (Fig. 7a–c, ii, respectively). However, both collections overestimate (bias median > 1.0) the total BA in group 4, the one with the most active fires (Fig. 7d, iv).

Here, we classified the CE into two types: a CE that occurs at the edge of the reference burned scars (CE_{EDGE}), to evaluate the overestimation of their area, and an isolated CE, which is considered a false alarm (CE_{FA}) (Libonati et al., 2015). The same procedure is applied to the OE: it is classified as a partial omission (OE_{EDGE}) when it refers to an underestimation of reference scar size, or it is classified as a total scar omission (OE_{SO}) when no portion of the burn is detected. As shown in Fig. 8a, CE_{FA} (Fig. 8a, i) and OE_{SO} (Fig. 8a, ii) are higher for lower levels of burning (Group 1) and lower for higher levels of burning (Group 4). The updated MCD64 algorithm provides reductions in the OE_{SO} of the detections of lower to high levels of burning (Group 1–4) at the same time that CE_{FA} increases for groups 1 and 2. A better insight into the characteristics of commission and omission errors is provided in Fig. 8b, which shows the proportion of each type of commissions (CE_{EDGE} and CE_{FA}) and omissions (OE_{EDGE} and OE_{SO}) errors. Fig. 8b(i) shows that CE_{FA} represents about 50% of CE in group 1 for both collections, with a successive decrease in the subsequent three groups (less than 22%). Comparing CE_{FA} between MCD64 collections, C6 presents a higher frequency than C5.1 for groups 1 and 2 (a surplus of 7% and 3%, respectively), the same frequency for group 3 and a lower frequency,

although minimal, of 1%, for group 4. On the other hand, the OE_{SO} are reduced in the C6, and the group 1 had the worst performance among the four groups (over 70%), with the following groups presenting OE_{SO} between 49% and 31% (Fig. 8b, ii). By analyzing the difference between the total edge errors (CE_{EDGE} and OE_{EDGE}) and the total isolated errors (CE_{FA} and OE_{SO}), we conclude that the errors of both collections are more associated with the underestimation/overestimation of the scar size, except for the low levels of burning represented by group 1.

Fig. 9 shows a local overview of the BA validation results for MCD64 C5.1 and C6 for four different regions over three Landsat path-rows located in the Southern Cerrado, namely, 219_074, 220_075, and 225_073, and for one located in the northern portion, 221_067. According to a visual inspection of Fig. 9, scars with large extensions and strong spectral signals are more easily identified, as expected. Smaller and fragmented scars are more difficult to detect, even with an area larger than the spatial resolution of the products. For instance, the 220_075 scene located in the southern Cerrado presents sugar cane plantation farms (Rudorff et al., 2010), where small and fast spreading fire fronts contribute to the BA omissions. On the other hand, in the 221_067 scene located in the northern Cerrado, which is characterized by large scars, C6 presents a small number of omission errors than C5.1. Overall, the updated algorithm captures more burned pixels, and the consistency between the C6 results and the reference scars was higher than for C5.1. The previous collection C5.1 is conservative, as a low level of CE is achieved at the expense of a high occurrence of OE. C6, in turn, has greater CE values with the majority of CE_{EDGE}, thus representing an overestimation of the size of the real scars, due to the low-resolution bias concept (Boschetti et al., 2004). In contrast, CE_{FA} in the strict sense represents the minority fraction of the CE. This drawback is common to other methods in the same region, as reported by Libonati et al. (2015).

Finally, we assessed the effect of land use on the estimated variability of C6 and C5.1 errors and patterns over the study region. Approximately 43% of the Cerrado biome belongs to some anthropogenic land cover, based on the MCD12Q1-IGBP C6 land-cover classification for 2015 and considering the Grasslands, Croplands and Cropland/Natural Vegetation Mosaic land cover classes. Fig. 10 shows the categorization of the study region into three degrees of LUI and reveals that low LUI, medium LUI, and high LUI occupy 56%, 26% and 18% of the study area analyzed, respectively. Regionally, 83% of the northern region is characterized as low-LUI, whereas in the southern region, medium- and high-LUI areas are predominant, accounting together for 76%.

A comparison between Figs. 3 and 10 reveals lower (higher) errors (for both C5.1 and C6) in areas with low (high) land use rates, highlighting the north-south contrasting patterns observed in Fig. 3. It is

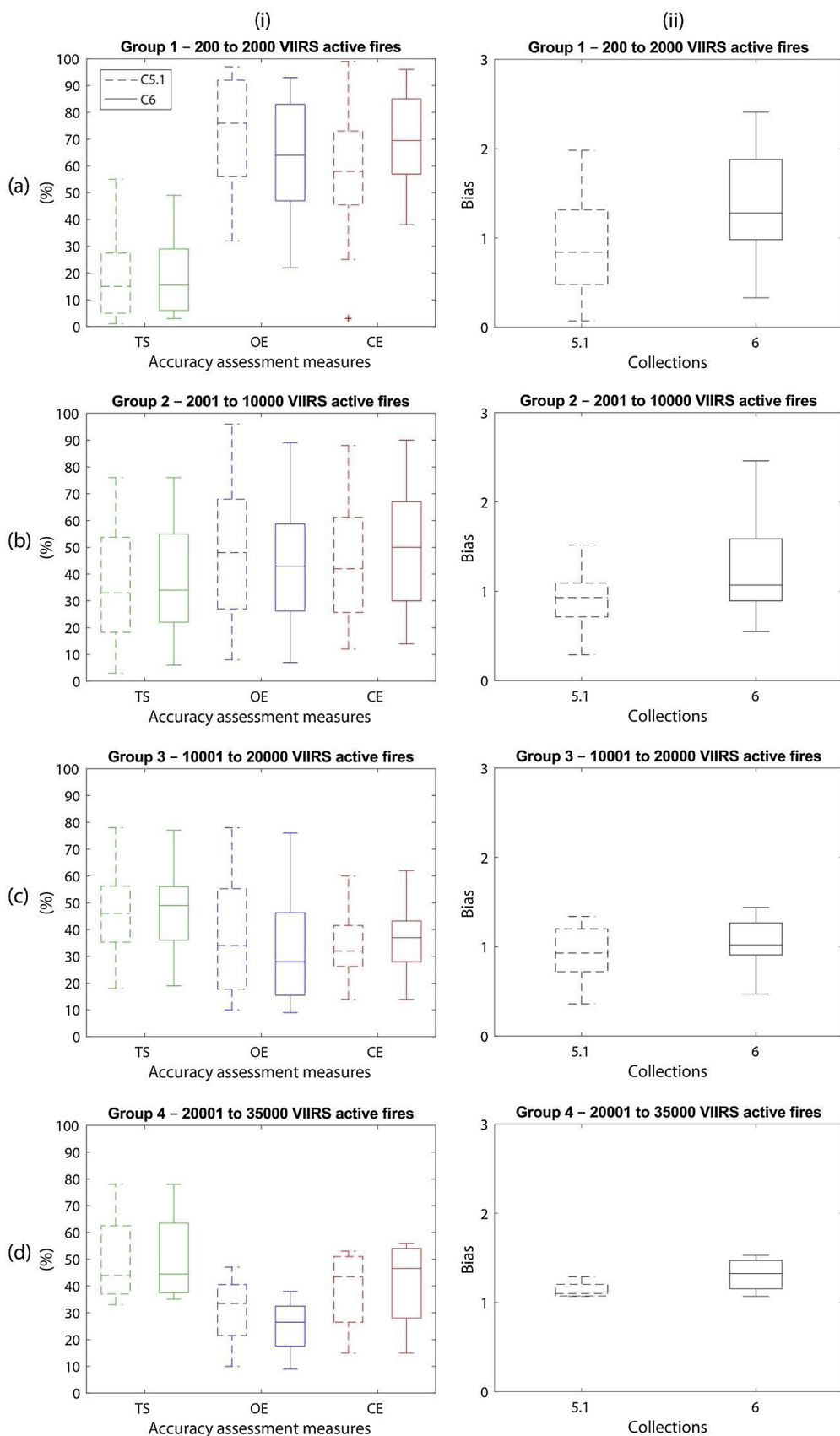


Fig. 7. Boxplots of the accuracy assessment measures (i) Threat Score – TS (green boxplots), Omission Error – OE (blue boxplots), Commission Error – CE (red boxplots) and (ii) Bias – B (black boxplots) for MCD64 C5.1 (dashed boxes) and MCD64 C6 (solid boxes). The results were categorized according to the classes in Fig. 4d: (a) Group 1 - 200–2000 VIIRS active fires, (b) Group 2 - 2001–10000 VIIRS active fires, (c) Group 3 - 10001–20000 VIIRS active fires and (d) Group 4 - 20001–35000 VIIRS active fires. (For interpretation of the references to colour in this figure legend, the reader is referred to the web version of this article).

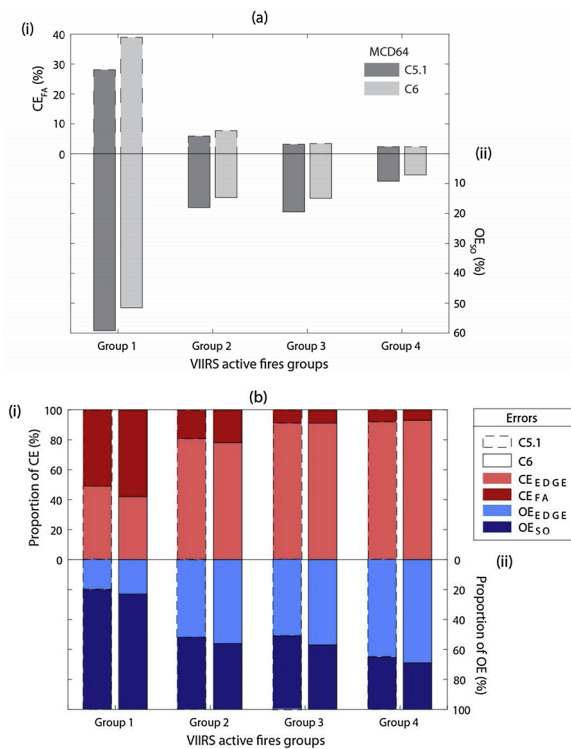


Fig. 8. (a) Frequency of CE_{FA} (% i, dashed bars) and frequency of OE_{SO} (% ii, solid bars) per VIIRS group for MCD64 C5.1 (dark gray bars) and MCD64 C6 (light gray bars). (b) Proportions of CE_{EDGE} (% i, light-red bars) and CE_{FA} (% i, red bars) and of OE_{EDGE} (% ii, light-blue bars) and OE_{SO} (% ii, dark-blue bars) per VIIRS group for MCD64 C5.1 (dashed bars) and MCD64 C6 (solid bars). (For interpretation of the references to colour in this figure legend, the reader is referred to the web version of this article).

worth noting that 95% of VIIRS group 1 – low amount of active fires (Fig. 4d) are observed in the southern part of the Cerrado biome, whereas groups 3 and 4 are observed only in the northern region. The north-south contrasting patterns regarding the amount of burned area and fire scar size and distribution are intrinsically related to land use intensity patterns, as observed in Fig. 10.

In this context, to understand the relationship between LUI and the occurrence of omission and commissions errors, we combined the observations from Figs. 3 and 10 into Table 2, which provides the total number of scenes in each combination of the land use levels (low, medium and high LUI) and OE and CE (intervals of 0–25%, 26–50%, 51–75% and 75–100%). Overall for C5.1, regions with low levels of LUI are associated with the predominance (63%) of smaller OE (i.e., OE < 50%). In contrast, for regions with high levels of LUI, the occurrence of higher OE (i.e., OE > 50%) is much greater (80%). Similar results were found in Russian croplands, where MCD64 C5.1 and MCD45 C5.1 missed the majority burned scars (Hall et al., 2016; Zhu et al., 2017) and in mountainous areas of China characterized by small fires (Fornacca et al., 2017). This limitation was reduced in C6, which exhibits a smaller predominance (73%) than C5.1 of higher OE (i.e., OE > 50%) for regions with high levels of LUI. In these regions, where fire scars typically are small and fragmented, C6 presents a reduction of the number of scenes presenting OE between 76–100% and an increase in the number of scenes presenting OE smaller than 25% compared to C5.1. For regions with low levels of LUI, the new collection C6 also exhibits improvements in the predominance (72%) of smaller OE (i.e., OE < 50%). Regarding the CE, the regions with low levels of LUI are more associated (65% of the cases for C5.1 and 63% of the cases for C6) with small CE (i.e., CE < 50%). In the regions with high levels of LUI, the number of scenes exhibiting high CE (i.e., CE > 50%) drastically increased in C6 (87% of the cases) compared to C5.1 (60% of the cases).

4. Discussion

The BA validation approach applied here is based on stratified samples that vary from very low (group 1) to high (group 4) numbers of active fire detections. In summary, our stratified analyses reveal that the accuracy assessment results of BA products vary according to the spatial configuration of the BA and the total amount, corroborating previous local studies conducted over the same region (Alves et al., 2018; Libonati et al., 2015). These results highlight how generalized samples may strongly influence the patterns of classification errors of BA products over a large coverage area (Boschetti et al., 2016; Padilla et al., 2017). Accordingly, these findings reveal the importance of taking into account the BA spatial variability for further global validation protocols, through the selection of stratified samples to guaranteeing the representativeness of the validation results.

The overall annual agreement between the spatial configuration of the total BA and the active fires was revealed to be high and stable ($\tau > 0.7$) in the studied area from 2013 to 2016, a period including extremely dry, extremely wet, and normal precipitation years. Several studies suggest that climate-fire relationships provide a general basis for understanding the natural seasonality and frequency of fire over the study region (Hoffmann et al., 2012; Nogueira et al., 2017a). Accordingly, we believe that our 2015 pixel-based validation using the Landsat images is representative of a diverse set of years, suggesting error-pattern stability. Nevertheless, other factors may also influence fire activity and may contribute to some variability, including political and economic drivers (Durigan and Ratter, 2016; Lapola et al., 2014).

The well-defined north-south gradient among the different accuracy measures is coincident with the largest scars and the largest amount of BAs (represented by the size of circles inside each L8 scene from Fig. 3) in the northern region. Greater inaccuracies from both collections are found in the south, which is characterized by small burned scars. These results are similar to previous studies showing that MCD64 C5.1 is unable to detect small fires in many other regions of the globe (Hall et al., 2016; Padilla et al., 2015; Wang et al., 2017; Zhu et al., 2017). Those patterns of error variability are related to the substantial heterogeneity in the temporal and spatial distribution of land use/cover and fire occurrence along the entire Cerrado biome, as already observed in previous studies using in situ and satellite datasets (Beuchle et al., 2015; Gomes et al., 2018).

These findings are in accordance with the predominance of less humanized areas in the northern portion of the Cerrado and a well-marked land conversion process in the southern region (Lapola et al., 2014). In the southern part of the Cerrado, natural vegetation has been converted into agriculture and cropland, both characterized by fragmented landscapes and small fires (Durigan and Ratter, 2016). In contrast, the northern region of the Cerrado has a higher concentration of conservation units and indigenous protected areas (Carranza et al., 2014; Mistry et al., 2005).

The Action Plan for Prevention and Control Deforestation and Fire in the Cerrado was recently implemented, recognizing the need for better conservation of the Cerrado biome (Beuchle et al., 2015). However, despite political efforts, the southern region of the Cerrado exhibited an increase of land conversion to pasture and agricultural areas in the last few decades, especially in the transition regions with the Pantanal and Atlantic Forest biomes. These transition areas may be mainly associated with sugarcane and soybean plantations, pasture and deforestation of secondary forest activities (Dias et al., 2016; Lapola et al., 2014; Song et al., 2018). The relation between BA and deforestation is still quite common, since fire, despite policies prohibiting its use, remains the primary tool for farmers to clean and open areas (Van Der Werf et al., 2010; van Marle et al., 2017). A study on land expansion for croplands and pasturelands throughout Latin America from 2001 to 2013 found that this practice led to deforestation in central Mato Grosso state and that new croplands came from non-forestland in the Cerrado (Graesser et al., 2015). The biome witnessed the most

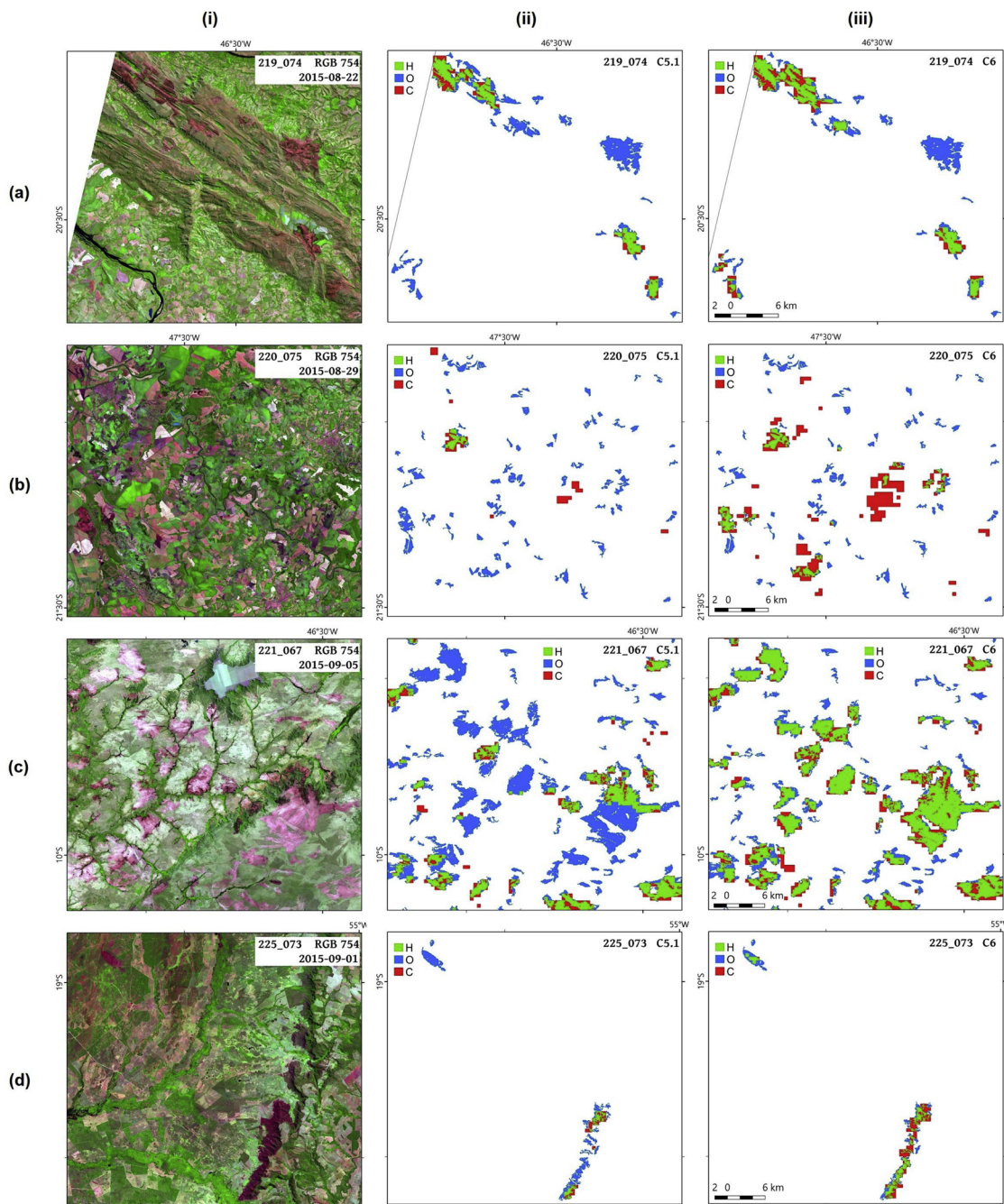


Fig. 9. Example MCD64 products accuracy assessment relative to the reference scars: (i) false-color RGB 754 Landsat composites showing burned scars in four Landsat scenes represented by the last date used for validation: (a) 219_074, (b) 220_075, (c) 221_067, and (d) 225_073. Comparison between the validation results from MCD64 C5.1 (ii) and C6 (iii), highlighting hints (H, green), omission (O, blue) and commission (C, red) errors. (For interpretation of the references to colour in this figure legend, the reader is referred to the web version of this article).

significant inclusion of new areas of croplands and pasturelands, with 9.96 Mha and 13 Mha, respectively, with the majority in southern states (Pivello, 2011).

Agricultural fires are still underestimated by satellite-derived products (Giglio et al., 2018), which are more accurate where spatial burned area patterns are extensive. Although the authors of the updated algorithm have observed in general more area burned with C6, there still are CE involved in the burned area quantification. This case can also be observed in this study, due to the high commission errors registered in the southern region of the Cerrado. The BAs resulting from prescribed fires associated with agricultural practices are underestimated even by medium-spatial-resolution satellite imagery such as

Landsat (Nowell et al., 2018).

Our results demonstrated an improvement of MCD64 C6 compared to C5.1 due to a decrease in OE values. These results are in accordance with previous studies stating that among the improvements of C6, the most substantial gain was in reducing the omission error by refining the BA detection (Giglio et al., 2018, 2016b). The overall improvement in BA detection from MCD64 C6 was also observed in recent studies comparing different BA mapping algorithms in South America (Chuvieco et al., 2018; Ramo et al., 2018), the Brazilian Amazon (Alves et al., 2018) and other regions worldwide (Wang et al., 2017; Zhu et al., 2017). For example, two recent studies have characterized the differences between C5.1 and C6 over a few areas of the Cerrado and found

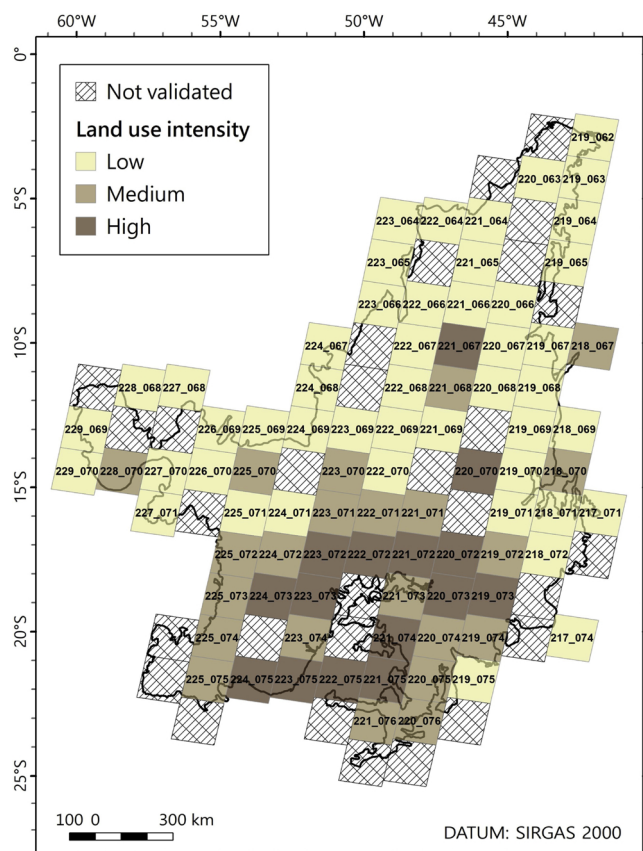


Fig. 10. Land use intensity distribution for 2015 in each path/row scene validated in the Brazilian Savannas (Cerrado). The dataset used for the land use intensity was derived from the MCD12Q1 C6 at a spatial resolution of 500 m. The colors represent the land use intensity occupying from 0 to 50% (low, yellow), 51–75% (medium, light brown) and 76–100% (high, dark brown) of each area belonging to the MCD12Q1 C6 land cover classes of Grasslands, Croplands, and Cropland/Natural Vegetation Mosaic from the IGBP classification. (For interpretation of the references to colour in this figure legend, the reader is referred to the web version of this article).

Table 2

Number of scenes in each level of land use (low, 0–50%; medium, 51–75%, and high, 76–100% of land use intensity (LUI) occupation from Fig. 10) and the omissions (OE) and commissions (CE) errors intervals (from 0 to 100% as in Fig. 3) for MCD64 C5.1 and MCD64 C6.

Number of scenes in each class of OE and LUI for C5.1 / C6	0-25%	26-50%	OE 51-75%	76-100%	Total
LUI Low	13 / 15	16 / 18	12 / 11	5 / 2	46
LUI Medium	1 / 2	7 / 10	9 / 7	6 / 4	23
LUI High	1 / 3	2 / 1	5 / 6	7 / 5	15
Total	15 / 20	25 / 29	26 / 24	18 / 11	84

Number of scenes in each class of CE and LUI for C5.1 / C6	0-25%	26-50%	CE 51-75%	76-100%	Total
LUI Low	11 / 8	19 / 21	11 / 12	5 / 5	46
LUI Medium	4 / 3	7 / 7	9 / 7	3 / 6	23
LUI High	3 / 0	3 / 2	7 / 7	2 / 6	15
Total	18 / 11	29 / 30	27 / 26	10 / 17	84

that the updated collection is better correlated with reference data than are the old collection and other global BA products (Alves et al., 2018; Giglio et al., 2018). It is worth noting that the difference between total BA from MCD64 C6 and C5.1 (C6-C5.1) is similar to the total BA detected by MCD45 C5.1, using only highly reliable observations (QF = 1; 5,900,040 ha). These results indicate that C6 is more effective in

detecting BA, in contrast to the MCD45 algorithm (Giglio et al., 2018). A comparison between the above BA values and results obtained with MCD45 C5.1 indicates that the latter only identified 48% of the total BA (Padilla et al., 2014) and detects 70% less BA than the reference datasets for the Cerrado (Libonati et al., 2015).

However, the reduction in OE is achieved at the expense of the CE enhancement since the concomitant reduction of both errors is viewed as conflicting due to the low-resolution bias concept (Boschetti et al., 2004). The CE associated with cloud masking in the reference images were reduced by using images with 10% or less cloud cover. Furthermore, the persistence time of the burned patches may be a limiting factor in the detection accuracy of the global-scale mapping (Pereira et al., 2017). However, the persistence time was taken into account in the 16-day period between the pairs of Landsat images. The median value of the persistence time for the predominant land cover classes in our study area (Fig. 1), – namely, savanna, woody savanna, and grassland – varies between 16 and 48 days, with little variability (Melchiorre and Boschetti, 2018).

The spatial gradient between the north and south regions observed in all results is not only due to the latitudinal variation leading to considerably different climatic regimes, but mainly due to the irregular and complex distribution of land cover and land use. Regions with greater native vegetation cover and lower land use intensity, such as the northern Cerrado, are vulnerable to fire propagation due to dry fuel accumulation in the dry season, with fires spreading into the neighboring native-vegetation areas. Therefore, the burned scars in these regions have larger areas and contiguous patterns, which favor remote sensing detection and consequently OE reduction. The fragmented pattern of burning in agriculture and pasture, in addition to soil management to clear land, hampers the good accuracy of low-spatial-resolution products for those areas (Laurent et al., 2018), as observed in the southern Cerrado.

The improvement of the C6 collection in detecting burned area is due to the use of more refined input data and the inclusion/modification of different parameters in the algorithm, combined with the empirical knowledge of the developers (Giglio et al., 2018). Briefly, the algorithm was adjusted in a manner that allowed: i) a reduction in grid cells that were unmapped due to lack of information, correction of cloud commissions and a shortened temporal window; ii) higher detection confidence in estimating the burn date, due to the shortened temporal window; iii) imposition of less-stringent thresholds to classify a pixel as burned; iv) reduction of the minimum likelihood threshold of the provisional classification to reduce the OE frequency; and v) application of a filter technique to reconsider the preliminary burn classification.

In this way, we can conclude that in the Cerrado biome, the general results for MCD64 C6 corroborate the a) considerable increase in the total burned area mapped, b) better performance in detecting small burnings, and c) OE (CE) reduction (increase) reported in the updated algorithm global validation disclosure (Giglio et al., 2018).

5. Conclusions and perspectives

Quantification of uncertainties from BA maps derived from orbital sensors, particularly the MCD64 product for the Brazilian Cerrado, such as that presented herein, have never been performed for the entire biome in a consistent manner. Our results indicate that uncertainties in BA retrieval using MCD64 in the Cerrado are most significant over the southern portion, consistent with previous studies that have found large uncertainties for BA products over specific areas located within this region (Giglio et al., 2018; Pereira et al., 2017). This limited accuracy of both versions of MCD64 in the southern Cerrado may be related to land-use dynamics associated with pasture and croplands, which use fire for land clearing, crop residue burning, and pasture renewal. In comparison, uncertainties in less human-disturbed regions are generally small, such as in the northern portion of Cerrado. We demonstrate that the

spatial pattern and extent of the burned patches are relatively easier to map and to quantify over the northern part of the Cerrado. Importantly, we note that changes in the development of the MCD64 algorithm, namely the updated MCD64 C6, contributed to detection improvements in small burn scar patches, although this enhancement tends to increase commission error. Thus, a comprehensive daily representation of fire regime in regions characterized by small and sparse burned scars, such as the Brazilian southern Cerrado, remains imperfect and may require higher image resolution, such as that provided by VIIRS I-band imagery.

The biome-level validation approach applied here can provide crucial insights into the regional understanding of fire regime uncertainties when remote sensing products are used, can supply model developers data and may be useful to reduce algorithm constraints or refining thresholds for mapping fire scars. Our results may also inform alternative approaches to BA mapping of small and fragmented scars from space. By successfully providing a quantification of the limitations of cutting-edge BA products over the entire Cerrado biome, this study motivates further research into the reliability of estimates of emissions from cropland burning applied in policy-making decisions. Understanding errors in the quantification of BAs may also ultimately lead to more robust regional future projections of fire regimes, which are crucial for adaptation and mitigation actions.

Funding

The study is funded by the Serrapilheira Institute (grant number Serra-1708-15159), by FAPESP (grants 2015/01389–4, 2015/50454-3) and by FCT (grant 1389/2014). RL is funded by CNPQ (grants 305159/2018-6 and 441971/2018-0). CEF is funded by Fundação para a Ciência e a Tecnologia I.P. (FCT), Portugal (UID/AGR/00239/2013) AAP is funded by CNPQ (grant 215158/2014-8).

References

- Alonso-Canas, I., Chuvieco, E., 2015. Global burned area mapping from ENVISAT-MERIS and MODIS active fire data. *Remote Sens. Environ.* 163, 140–152. <https://doi.org/10.1016/j.rse.2015.03.011>.
- Alvares, C.A., Stape, L., Sentelhas, P.C., Gonçalves, L.D.M., Sparovek, G., 2014. Köppen's climate classification map for Brazil. *Clayton. Meteorol. Zeitschrift* 22, 711–728. <https://doi.org/10.1127/0941-2948/2013/0507>.
- Alves, D.B., Pérez-Cabello, F., Febrer-Martínez, M., 2018. Accuracy assessment of the latest generations of MODIS burned area products for mapping fire scars on a regional scale over Campos Amazônicos Savanna Enclave (Brazilian Amazon). *J. Appl. Remote Sens.* 12, 026026-1–026026-21. <https://doi.org/10.1117/1.JRS.12.026026>.
- Andela, N., Morton, D.C., Giglio, L., Chen, Y., Van Der Werf, G.R., Kasibhatla, P.S., DeFries, R.S., Collatz, G.J., Hantson, S., Kloster, S., Bachelet, D., Forrest, M., Lasslop, G., Li, F., Mameon, S., Melton, J.R., Yue, C., Randerson, J.T., 2017. A human-driven decline in global burned area. *Science* (80-) 356, 1356–1362. <https://doi.org/10.1126/science.aal4108>.
- Araújo, F.M., De Ferreira, L.G., 2015. Satellite-based automated burned area detection: a performance assessment of the MODIS MCD45A1 in the Brazilian savanna. *Int. J. Appl. Earth Obs. Geoinf.* 36, 94–102. <https://doi.org/10.1016/j.jag.2014.10.009>.
- Araújo, F.M., Ferreira, L.G., Arantes, A.E., 2012. Distribution patterns of burned areas in the Brazilian biomes: an analysis based on satellite data for the 2002–2010 period. *Remote Sens.* 4, 1929–1946. <https://doi.org/10.3390/rs4071929>.
- Archibald, S., Lehmann, C.E.R., 2018. Biological and geophysical feedbacks with fire in the Earth system. *Environ. Res. Lett.* 1361471480.
- Beerling, D.J., Osborne, C.P., 2006. The origin of the savanna biome. *Glob. Change Biol.* 12, 2023–2031. <https://doi.org/10.1111/j.1365-2486.2006.01239.x>.
- Beuchle, R., Grecchi, R.C., Shimabukuro, Y.E., Seliger, R., Eva, H.D., Sano, E., Achard, F., 2015. Land cover changes in the Brazilian Cerrado and Caatinga biomes from 1990 to 2010 based on a systematic remote sensing sampling approach. *Appl. Geogr.* 58, 116–127. <https://doi.org/10.1016/j.apgeog.2015.01.017>.
- Boschetti, L., Flasse, S.P., Brivio, P.A., 2004. Analysis of the conflict between omission and commission in low spatial resolution dichotomic thematic products: the Pareto Boundary. *Remote Sens. Environ.* 91, 280–292. <https://doi.org/10.1016/j.rse.2004.02.015>.
- Boschetti, M., Stroppiana, D., Brivio, P.A., 2010. Mapping burned areas in a Mediterranean environment using soft integration of spectral indices from high-resolution satellite images. *Earth Interact.* 14. <https://doi.org/10.1175/2010EI349.1>.
- Boschetti, L., Roy, D.P., Justice, C.O., Humber, M.L., 2015. MODIS-Landsat fusion for large area 30m burned area mapping. *Remote Sens. Environ.* 161, 27–42. <https://doi.org/10.1016/j.rse.2015.01.022>.
- Boschetti, L., Stehman, S.V., Roy, D.P., 2016. A stratified random sampling design in space and time for regional to global scale burned area product validation. *Remote Sens. Environ.* 186, 465–478. <https://doi.org/10.1016/j.rse.2016.09.016>.
- Carranza, T., Balmford, A., Kapos, V., Manica, A., 2014. Protected area effectiveness in reducing conversion in a rapidly vanishing ecosystem: The Brazilian Cerrado. *Conserv. Lett.* 7, 216–223. <https://doi.org/10.1111/conl.12049>.
- Chen, Y., Morton, D.C., Jin, Y., Collatz, G.J., Prasad, S., Werf, G.R., Van Der Defries, R.S., Randerson, J.T., Chen, Y., Morton, D.C., Jin, Y., Collatz, G.J., Prasad, S., 2013a. Long-term trends and interannual variability of forest, savanna and agricultural fires in South America. *Carbon Manag.* 3004, 617–638. <https://doi.org/10.4155/cmt.13.61>.
- Chen, Y., Morton, D.C., Jin, Y., Gollatz, G.J., Kasibhatla, P.S., Van Der Werf, G.R., Defries, R.S., Randerson, J.T., 2013b. Long-term trends and interannual variability of forest, savanna and agricultural fires in South America. *Carbon Manag.* 4, 617–638. <https://doi.org/10.4155/cmt.13.61>.
- Chuvieco, E., Opazo, S., Sione, W., Del Valle, H., Anaya, J., Di Bella, C., Cruz, I., Manzo, L., López, G., Mari, N., González-Alonso, F., Morelli, F., Setzer, A., Csizsar, I., Kanpandegi, J.A., Bastarrika, A., Libonati, R., 2008. Global burned-land estimation in Latin America using MODIS composite data. *Ecol. Appl.* 18, 64–79. <https://doi.org/10.1890/06-2148.1>.
- Chuvieco, E., Martínez, S., Román, M.V., Hantson, S., Pettinari, M.L., 2014. Integration of ecological and socio-economic factors to assess global vulnerability to wildfire. *Glob. Ecol. Biogeogr.* 23, 245–258. <https://doi.org/10.1111/geb.12095>.
- Chuvieco, E., Lizundia-loiola, J., Pettinari, M.L., Ramo, R., Padilla, M., Mouillot, F., Laurent, P., Storm, T., Heil, A., Plummer, S., 2018. Generation and analysis of a new global burned area product based on MODIS 250m reflectance bands and thermal anomalies. *Earth Syst. Sci. Data Discuss* 512, 1–24.
- Csizar, I., Schroeder, W., Giglio, L., Ellicott, E., Vadrevu, K.P., Justice, C.O., Wind, B., 2014. Active fires from the suomi NPP visible infrared imaging radiometer suite: Product status and first evaluation results. *J. Geophys. Res.* 119, 803–816. <https://doi.org/10.1002/2013JD020453>.
- Dantas, D.L., Pausas, J.G., Batalha, M., Loiola, P., Cianciaruso, M., 2013. The role of fire in structuring trait variability in Neotropical savannas. *Oecologia* 171, 487–494. <https://doi.org/10.1007/s00442-012-2431-8>.
- DaSilva, J., Bates, J., 2002. Biogeographic patterns and conservation in the South American Cerrado: a tropical Savanna hotspot. *BioOne* 52, 225–234.
- Dias, L.C.P., Pimenta, F.M., Santos, A.B., Costa, M.H., Ladle, R.J., 2016. Patterns of land use, extensification, and intensification of Brazilian agriculture. *Glob. Change Biol.* 22, 2887–2903. <https://doi.org/10.1111/gcb.13314>.
- Durigan, G., Ratter, J.A., 2016. The need for a consistent fire policy for Cerrado conservation. *J. Appl. Ecol.* 53, 11–15. <https://doi.org/10.1111/1365-2664.12559>.
- Fornacca, D., Ren, G., Xiao, W., 2017. Performance of Three MODIS Fire Products (MCD45A1, MCD64A1, MCD14ML), and ESA Fire_CCI in a Mountainous Area of Northwest Yunnan, China, Characterized by Frequent Small Fires. *Remote Sens.* 9, 1131. <https://doi.org/10.3390/rs9111131>.
- Franco, A.C., Rossatto, D.R., de Carvalho Ramos Silva, L., da Silva Ferreira, C., 2014. Cerrado vegetation and global change: the role of functional types, resource availability and disturbance in regulating plant community responses to rising CO2 levels and climate warming. *Theor. Exp. Plant Physiol.* 26, 19–38. <https://doi.org/10.1007/s40626-014-0002-6>.
- Friedl, M.A., Sulla-Menashe, D., Tan, B., Schneider, A., Ramankutty, N., Sibley, A., Huang, X., 2010. MODIS Collection 5 global land cover: algorithm refinements and characterization of new datasets. *Remote Sens. Environ.* 114, 168–182.
- Giglio, L., Loboda, T., Roy, D.P., Quayle, B., Justice, C.O., 2009. An active-fire based burned area mapping algorithm for the MODIS sensor. *Remote Sens. Environ.* 113, 408–420. <https://doi.org/10.1016/j.rse.2008.10.006>.
- Giglio, L., Randerson, J.T., Van Der Werf, G.R., Kasibhatla, P.S., Collatz, G.J., Morton, D.C., Defries, R.S., 2010. Assessing variability and long-term trends in burned area by merging multiple satellite fire products. *Biogeosciences* 7, 1171–1186. <https://doi.org/10.5194/bg-7-1171-2010>.
- Giglio, L., Boschetti, L., Roy, D., Hoffman, A.A., Humber, M., 2016a. Collection 6 MODIS burned area product user guide version 1. *Nasa Version 1*, 1–12.
- Giglio, L., Schroeder, W., Justice, C.O., 2016b. The collection 6 MODIS active fire detection algorithm and fire products. *Remote Sens. Environ.* 178, 31–41. <https://doi.org/10.1016/j.rse.2016.02.054>.
- Giglio, L., Boschetti, L., Roy, D.P., Humber, M.L., Justice, C.O., 2018. The Collection 6 MODIS burned area mapping algorithm and product. *Remote Sens. Environ.* 217, 72–85. <https://doi.org/10.1016/j.rse.2018.08.005>.
- Gomes, L., Miranda, H.S., Bustamante, M.M., da, C., 2018. How can we advance the knowledge on the behavior and effects of fire in the Cerrado biome? *For. Ecol. Manage.* 417, 281–290. <https://doi.org/10.1016/J.FORECO.2018.02.032>.
- Graesser, J., Aide, T.M., Grau, H.R., Ramankutty, N., 2015. Cropland/pastureland dynamics and the slowdown of deforestation in Latin America. *Environ. Res. Lett.* 10. <https://doi.org/10.1088/1748-9326/10/3/034017>.
- Hall, J.V., Loboda, T.V., Giglio, L., McCarty, G.W., 2016. A MODIS-based burned area assessment for Russian croplands: mapping requirements and challenges. *Remote Sens. Environ.* 184, 506–521. <https://doi.org/10.1016/J.RSE.2016.07.022>.
- Hantson, S., Armeth, A., Harrison, S., Kelley, D., Prentice, I., Rabin, S., Archibald, S., Mouillot, F., Arnold, R., Artaxo, P., Ciais, P., Hickler, T., 2016. The status and challenge of global fire modelling. *Biogeosci. Discuss.* 13, 3359–3375. <https://doi.org/10.5194/bg-2016-17>.
- Hoffmann, W., 2002. Positive feedbacks of fire, climate, and vegetation and the conversion of tropical savanna. *Geophys. Res. Lett.* 29, 5–8. <https://doi.org/10.1029/2002GL015424>.
- Hoffmann, W.A., Jaconis, S.Y., Mckinley, K.L., Geiger, E.L., Gotsch, S.G., Franco, A.C.,

2012. Fuels or microclimate? Understanding the drivers of fire feedbacks at savanna-forest boundaries. *Austral Ecol.* 37, 634–643. <https://doi.org/10.1111/j.1442-9993.2011.02324.x>.
- Humber, M.L., Boschetti, L., Giglio, L., Justice, C.O., 2018. Spatial and temporal inter-comparison of four global burned area products. *Int. J. Digit. Earth* 1–25. <https://doi.org/10.1080/17538947.2018.1433727>.
- Klink, C.A., Machado, R.B., 2005. Conservation of the Brazilian Cerrado. *Conserv. Biol.* 19, 707–713. <https://doi.org/10.1111/j.1523-1739.2005.00702.x>.
- Kottek, M., Grieser, J., Beck, C., Rudolf, B., Rubel, F., 2006. World map of the Köppen-Geiger climate classification updated. *Meteorol. Zeitschrift* 15, 259–263. <https://doi.org/10.1127/0941-2948/2006/0130>.
- Lapola, D.M., Martinelli, L.A., Peres, C.A., Ometto, J.P.H.B., Ferreira, M.E., Nobre, C.A., Aguiar, A.P.D., Bustamante, M.M.C., Cardoso, M.F., Costa, M.H., Joly, C.A., Leite, C.C., Moutinho, P., Sampaio, G., Strassburg, B.B.N., Vieira, I.C.G., 2014. Pervasive transition of the Brazilian land-use system. *Nat. Clim. Change* 4, 27–35. <https://doi.org/10.1038/nclimate2056>.
- Laurent, P., Mouillot, F., Yue, C., Ciais, P., Moreno, M.V., Nogueira, J.M.P., 2018. Data Descriptor: FRY, a global database of fire patch functional traits derived from spaceborne burned area products. *Sci. Data* 5, 1–12. <https://doi.org/10.1038/sdata.2018.132>.
- Libonati, R., DaCamara, C.C., Setzer, A.W., Morelli, F., Melchiori, A.E., 2015. An algorithm for burned area detection in the Brazilian Cerrado using 4 µm MODIS imagery. *Remote Sens.* 7, 15782–15803. <https://doi.org/10.3390/rs71115782>.
- Lillesand, T.M., Kiefer, R.W., 1994. *Remote Sensing and Photo Interpretation*. John Wiley Sons, New York, pp. 750.
- Loveland, T.R., Belward, A.S., 1997. The IGBP-dis global 1km land cover data set, discover: first results. *Int. J. Remote Sens.* 18, 3289–3295. <https://doi.org/10.1080/014311697217099>.
- Melchiori, A.E., Setzer, A.W., Morelli, F., Libonati, R., Cândido, P., de, A., de Jesus, S.C., 2014. A Landsat-TM/OLI algorithm for burned areas in the Brazilian Cerrado: preliminary results. *Adv. For. fire Res.* 23–30.
- Melchiorre, A., Boschetti, L., 2018. Global analysis of burned area persistence time with MODIS data. *Remote Sens.* 10, 750. <https://doi.org/10.3390/rs10050750>.
- Miranda, H.S., Sato, M.N., Neto, W.N., Aires, F.S., 2009. Fires in the cerrado, the Brazilian savanna. *Tropical Fire Ecology*. Springer, Berlin Heidelberg, Berlin, Heidelberg, pp. 427–450. https://doi.org/10.1007/978-3-540-77381-8_15.
- Mistry, J., Berardi, A., Andrade, V., Krahô, T., Krahô, P., Leonardos, O., 2005. Indigenous fire management in the cerrado of Brazil: the case of the Krahô of Tocantins. *Hum. Ecol.* 33, 365–386. <https://doi.org/10.1007/s10745-005-4143-8>.
- Mouillot, F., Schultz, M.G., Yue, C., Cadule, P., Tansey, K., Ciais, P., Chuvieco, E., 2014. Ten years of global burned area products from spaceborne remote sensing-A review: Analysis of user needs and recommendations for future developments. *Int. J. Appl. Earth Obs. Geoinf.* <https://doi.org/10.1016/j.jag.2013.05.014>.
- Myers, N., Mittermeier, R.A., Mittermeier, C.G., Da Fonseca, G.A.B., Kent, J., 2000. Biodiversity hotspots for conservation priorities. *Nature* 403, 853–858.
- Nogueira, J., Rambal, S., Mouillot, F., 2017a. Spatial pattern of the seasonal drought / burned area relationship across Brazilian biomes: sensitivity to drought metrics and global remote-sensing fire products. *Climate* 5. <https://doi.org/10.3390/cli5020042>.
- Nogueira, J., Ruffault, J., Chuvieco, E., Mouillot, F., 2017b. Can we go beyond burned area in the assessment of global remote sensing products with fire patch metrics? *Remote Sens.* 9, 7. <https://doi.org/10.3390/rs9010007>.
- Nowell, H., Homes, C., Robertson, K., Teske, C., Hiers, J., 2018. A new picture of fire extent, variability, and drought interaction in prescribed fire landscapes: insights from florida government records. *Geophys. Res. Lett.* 45, 7874–7884. <https://doi.org/10.1029/2018GL078679>.
- Oliva, P., Schroeder, W., 2015. Assessment of VIIRS 375m active fire detection product for direct burned area mapping. *Remote Sens. Environ.* 160, 144–155. <https://doi.org/10.1016/j.rse.2015.01.010>.
- Padilla, M., Stehman, S.V., Chuvieco, E., 2014. Validation of the 2008 MODIS-MCD45 global burned area product using stratified random sampling. *Remote Sens. Environ.* 144, 187–196. <https://doi.org/10.1016/j.rse.2014.01.008>.
- Padilla, M., Stehman, S.V., Ramo, R., Corti, D., Hantson, S., Oliva, P., Alonso-Canas, I., Bradley, A.V., Tansey, K., Mota, B., Pereira, J.M., Chuvieco, E., 2015. Comparing the accuracies of remote sensing global burned area products using stratified random sampling and estimation. *Remote Sens. Environ.* 160, 114–121. <https://doi.org/10.1016/j.rse.2015.01.005>.
- Padilla, M., Olofsson, P., Stehman, S.V., Tansey, K., Chuvieco, E., 2017. Stratification and sample allocation for reference burned area data. *Remote Sens. Environ.* 203, 240–255. <https://doi.org/10.1016/j.rse.2017.06.041>.
- Panisset, J., Dacamara, C.C., Libonati, R., Peres, L.F., Calado, T.J., Barros, A., 2017. Assigning dates and identifying areas affected by fires in Portugal based on MODIS data. *An. Acad. Bras. Cienc.* 89. <https://doi.org/10.1590/0001-3765201720160707>.
- Pereira, A., Pereira, J.M.C., Libonati, R., Oom, D., Setzer, A.W., Morelli, F., Machado-Silva, F., de Carvalho, L.M.T., 2017. Burned area mapping in the Brazilian Savanna using a one-class support vector machine trained by active fires. *Remote Sens.* 9. <https://doi.org/10.3390/rs9111161>.
- Pivello, V.R., 2011. The use of fire in the cerrado and Amazonian rainforests of Brazil: past and present. *Fire Ecol.* 7, 24–39. <https://doi.org/10.4996/fireecology.0701024>.
- Pivello, V.R., 2017. Fire Management for Biological Conservation in the Brazilian Cerrado. pp. 141–166. <https://doi.org/10.4324/9781315243788-14>.
- Ramo, R., Chuvieco, E., 2017. Developing a random forest algorithm for MODIS global burned area classification. *Remote Sens.* 9, 1193. <https://doi.org/10.3390/rs911193>.
- Ramo, R., Rodríguez, D., Chuvieco, E., 2018. A data mining approach for global burned area mapping. *Int. J. Appl. Earth Obs. Geoinf.* 73, 39–51. <https://doi.org/10.1016/j.jag.2018.05.027>.
- Randerson, J.T., Chen, Y., van der Werf, G.R., Rogers, B.M., Morton, D.C., 2012. Global burned area and biomass burning emissions from small fires. *J. Geophys. Res. Biogeosci.* 117. <https://doi.org/10.1029/2012JG002128>. n/a-n/a.
- Ratter, J., Ribeiro, J., Bridgewater, S., 1997. The Brazilian Cerrado Vegetation and Threats to its Biodiversity. *Ann. Geophys.* 80, 223–230.
- Roy, D.P., Giglio, L., Kendall, J.D., 1999. Multi-temporal active-fire based burn scar detection algorithm. *J. Int. J. Remote Sens.* 20, 20771.
- Roy, D.P., Jin, Y., Lewis, P.E., Justice, C.O., 2005. Prototyping a global algorithm for systematic fire-affected area mapping using MODIS time series data. *Remote Sens. Environ.* 97, 137–162. <https://doi.org/10.1016/j.rse.2005.04.007>.
- Roy, D., Roy, D., Boschetti, L., Boschetti, L., 2008. MODIS Collection 5 Burned Area Product MCD45. User Guid. Version 1. pp. 1–12.
- Rudorff, B.F.T., Aguiar, D.A., De Fernando, W., Sugawara, L.M., Adami, M., Moreira, M.A., 2010. Studies on the Rapid Expansion of Sugarcane for Ethanol Production in São Paulo State (Brazil) Using Landsat Data 1057–1076. <https://doi.org/10.3390/rs2041057>.
- Sano, E.E., Rosa, R., Brito, J.L.S., Ferreira, L.G., 2010. Land cover mapping of the tropical savanna region in Brazil. *Env. Monit Assess* 116, 113–124. <https://doi.org/10.1007/s10661-009-0988-4>.
- Santín, C., Doerr, S.H., 2016. Fire effects on soils: the human dimension. *Philos. Trans. R. Soc. Lond. B Biol. Sci.* 371. <https://doi.org/10.1098/rstb.2015.0171>.
- Santos, J.F.C., Romeiro, J.M.N., de Assis, J.B., Torres, F.T.P., Gleriani, J.M., 2018. Potentials and limitations of remote fire monitoring in protected areas. *Sci. Total Environ.* 616–617, 1347–1355. <https://doi.org/10.1016/J.SCITOTENV.2017.10.182>.
- Schroeder, W., Csizsar, I., Morisette, J., 2008. Quantifying the impact of cloud obscuration on remote sensing of active fires in the Brazilian Amazon. *Remote Sens. Environ.* 112, 456–470. <https://doi.org/10.1016/j.rse.2007.05.004>.
- Schroeder, W., Oliva, P., Giglio, L., Csizsar, I.A., 2014. The New VIIRS 375m active fire detection data product: algorithm description and initial assessment. *Remote Sens. Environ.* <https://doi.org/10.1016/j.rse.2013.12.008>.
- Silva, P., Bastos, A., DaCamara, C.C., Libonati, R., 2016. Future projections of fire occurrence in Brazil using EC-earth climate model. *Rev. Bras. Meteorol.* 31, 288–297. <https://doi.org/10.1590/0102-778631320150142>.
- Song, X.-P., Hansen, M.C., Stehman, S.V., Potapov, P.V., Tyukavina, A., Vermote, E.F., Townshend, J.R., 2018. Global land change from 1982 to 2016. *Nature*. <https://doi.org/10.1038/s41586-018-0411-9>.
- Strassburg, B.B.N., Brooks, T., Feltran-Barbieri, R., Iribarrem, A., Crouzeilles, R., Loyola, R., Latawiec, A.E., Oliveira Filho, F.J.B., De Scaramuzza, C.A.M., Scarano, F.R., Soares-Filho, B., Balmford, A., 2017. Moment of truth for the Cerrado hotspot. *Nat. Ecol. Evol.* 1, 1–3. <https://doi.org/10.1038/s41559-017-0099>.
- Sulla-Menashe, D., Friedl, M.A., 2018. User Guide to Collection 6 MODIS Land Cover (MCD12Q1 and MCD12C1) Product. pp. 1–18.
- Tsela, P.L., Van Helden, P., Frost, P., Wessels, K., Archibald, S., 2010. Validation of the modis burned-area products across different biomes in South Africa. *Int. Geosci. Remote Sens. Symp.* 3652–3655. <https://doi.org/10.1109/IGARSS.2010.5650253>.
- Tsela, P., Wessels, K., Botai, J., Archibald, S., Swanepoel, D., Steenkamp, K., Frost, P., 2014. Validation of the two standard MODIS satellite burned-area products and an empirically-derived merged product in South Africa. *Remote Sens.* 6, 1275–1293. <https://doi.org/10.3390/rs6021275>.
- Van Der Werf, G.R., Randerson, J.T., Giglio, L., Collatz, G.J., Mu, M., Kasibhatla, P.S., Morton, D.C., Defries, R.S., Jin, Y., Van Leeuwen, T.T., 2010. Global fire emissions and the contribution of deforestation, savanna, forest, agricultural, and peat fires (1997–2009). *Atmos. Chem. Phys.* 10, 11707–11735. <https://doi.org/10.5194/acp-10-11707-2010>.
- van Marle, M.J.E., Field, R.D., van der Werf, G.R., Estrada de Wagt, I.A., Houghton, R.A., Rizzo, L.V., Artaxo, P., Tsigaridis, K., 2017. Fire and deforestation dynamics in Amazonia (1973–2014). *Global Biogeochem. Cycles* 31, 24–38. <https://doi.org/10.1002/2016GB005445>.
- Wang, W., Cao, C., Bai, Y., Blonski, S., Schull, M.A., 2017. Assessment of the NOAA S-NPP VIIRS geolocation reprocessing improvements. *Remote Sens.* 9. <https://doi.org/10.3390/rs9100974>.
- Wilks, D.S., 2011. Statistical methods in the atmospheric sciences. *Int. Geophys. Ser.* <https://doi.org/10.1002/met.16>.
- Zhang, Y., Qin, D., Yuan, W., Jia, B., 2016. Historical trends of forest fires and carbon emissions in China from 1988 to 2012. *J. Geophys. Res. Biogeosci.* <https://doi.org/10.1002/2016JG003570>.
- Zhu, C., Kobayashi, H., Kanaya, Y., Saito, M., 2017. Size-dependent validation of MODIS MCD64A1 burned area over six vegetation types in boreal Eurasia: large underestimation in croplands. *Sci. Rep.* 7, 4181. <https://doi.org/10.1038/s41598-017-03739-0>.